HiSST: 3rd International Conference on
High-Speed Vehicle Science Technology
14 -19 April 2024, Busan, Korea

Establishment of Free Piston Type Expansion Tunnel

Honhar Gupta[1], Jithin Sreekumar[2], Mohammed Ibrahim Sugarno[3]

Abstract

In response to the growing need for ground test facilities for flow conditions corresponding to the re-entry of spacecraft in the planetary atmosphere, a Free Piston Type Hypersonic Expansion Tunnel (S2) is being established at the Hypersonic Experimental Aerodynamic Laboratory at IIT Kanpur. An expansion tunnel is an impulse facility that uses the enthalpy increment phenomenon of unsteady expansion. Free Piston Type Expansion Tunnel is 25.2 m long and has a nozzle exit diameter of 0.2 m. Test time vary according to flow conditions but typically are the order of 50 microseconds. Computational tools, high-frequency static and pitot pressure measurements using PCB pressure transducer, and Flow visualization using a High-speed camera are utilized for the characterization of flow conditions during test time. This facility is designed for stagnation enthalpies up to 40 MJ/Kg and flow velocity up to 8 km/s. Some experiments corresponding to one of the operating conditions have been performed in this study.

Keywords: *Expansion Tunnel, Hypersonic Flows, Free Piston Driver, Impulse facility*

Nomenclature

Latin
p – Pressure
Re – Reynolds Number
T – Temperature
M – Mach number
V – Velocity
H – Stagnation Enthalpy
a – Speed of sound
Greek
γ – Ratio of specific heat
ρ – density
Subscript
0 – Stagnation property
8 – Freestream property (after nozzle exit)
7 – Test gas property at nozzle inlet
6 – Property of shock-processed acceleration tube gas

1. Introduction

With the increase in interest in planetary entry and re-entry in Earth's atmosphere, ground based facilities present in the country are not sufficient to test the aerothermodynamics of space vehicles. Studies on missions involving Mars entry and Earth re-entry have found velocities of spacecraft up to 14 km/s within the atmosphere[1]. Shock tunnel can also produce the shock speed necessary for re-entry of the vehicle but all the energy is imparted to test gas across shock wave which can induce dissociation of test gas, rendering it unsuitable for testing. As a result, the Free Piston Type Expansion Tunnel is built to satisfy the country's rising demands. Expansion tunnel uses low pressure acceleration tube to unsteadily expand test gas to hypervelocity flow due to which flow has lower static temperature and less dissociation of test gas in comparison with a shock tunnel.

The concept of an expansion tunnel was first proposed by Resler and Bloxsom in 1952[2]. Operations of expansion tunnel theoretically were first described by Trimpi[3]. A number of these facilities has

[1] *PhD Scholar, Indian Institute of Technology Kanpur, nigotia.honhar@gmail.com*
[2] *PhD Scholar, Indian Institute of Technology Kanpur, jithinsreekumar1@gmail.com*
[3] *Associate Professor, Indian Institute of Technology Kanpur, ibrahim@iitk.ac.in*

been developedThe Langley 6-in. expansion tube pioneered by NASA Langley was the first expansion tube which was used as a facility for experiments[4]. This tunnel was later moved to GASL and commissioned as HYPULSE Facility. To heat the driver gas, Free piston was used first time by Stalker in the free piston shock tunnel in early 1960s[5]. First Free Piston type expansion tunnel was first built at the University of Queensland (UQ) by converting TQ shock tube in 1987[6]. Later many Expansion tunnel facilities were set up around the world such as X-series facilities at the University of Queensland[7], Hypervelocity Expansion Tunnel (HET) at CalTech[8], Michigan Hypersonic Expansion Tube Facility (MHExT) at the University of Michigan[9].

The present work describes the characterization of the newly developed Free Piston Type Expansion Tunnel (S2). This facility is designed for flow velocity up to 8 km/s and stagnation enthalpies up to 40 MJ/Kg. Currently, few experiments have been done to characterize the facility. More experiments are needed to fully calibrate the facility.

2. Overview and Operation of Expansion Tunnel

Schematic and picture of Free piston type expansion tunnel (FPET) are given in Fig. 1 and Fig. 2 respectively. The expansion tunnel consists of four sections- reservoir, driver tube, shock tube, and acceleration tube. The acceleration tube is connected to a dump tank test section via a nozzle. Free piston driver is generally filled with a mixture of helium and argon but in the current study air has been used as driver gas. The shock tube and acceleration tube are filled with air. The driver and shock tube are separated by an aluminum diaphragm (primary diaphragm) and the shock tube and acceleration tube are separated by mylar diaphragm (secondary diaphragm). The expansion tunnel is 25.2 m long and it uses an 18.3 kg piston. The nozzle exit diameter is 0.2 m. Dimensions of each part of the facility are presented in Table 1.

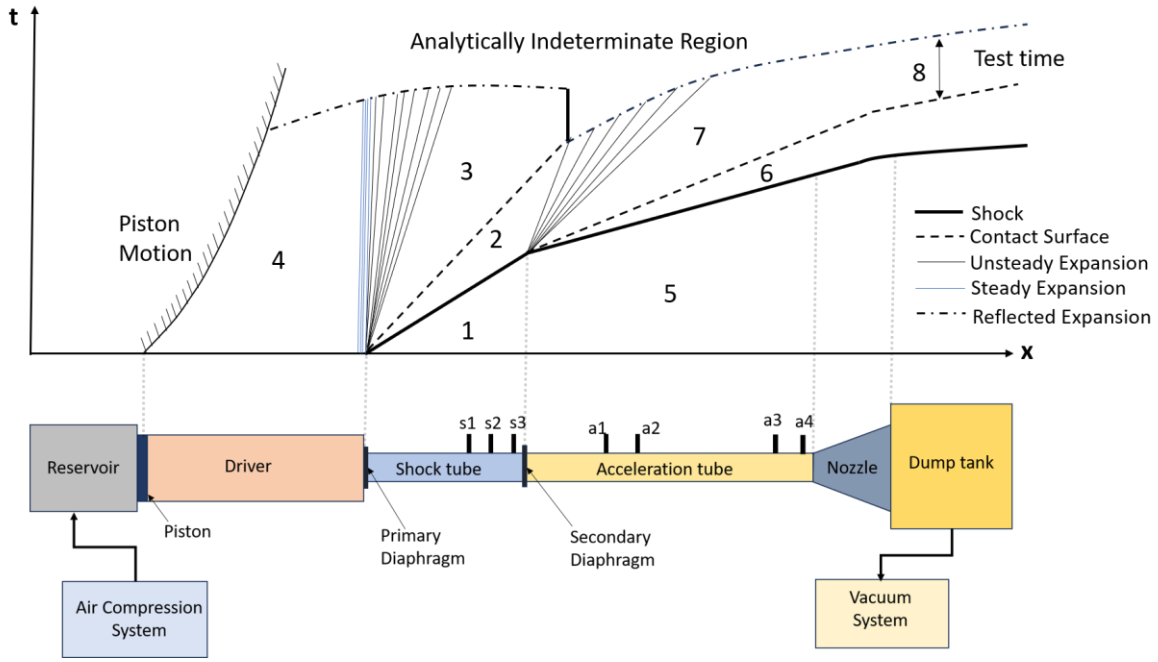

Fig 1. Schematic and Idealized distance-time (x-t) diagram of FPET (S2) (x-t diagram is not to scale)

To protect the facility from the impact of the piston; the reservoir, driver, shock tube, acceleration tube, and dump tank are placed on movable mounts. The maximum pressure that can be used in the reservoir is 40 bar.

Table 1. Dimensions of each part of FPET

Part	Size
Air Reservoir	Volume 0.1864 m^3
Driver Tube	Φ220 ✕ 6030 mm
Shock Tube	Φ65 ✕ 4500 mm
Acceleration Tube	Φ65 ✕ 8000 mm
Piston	Φ220 ✕ 200 mm

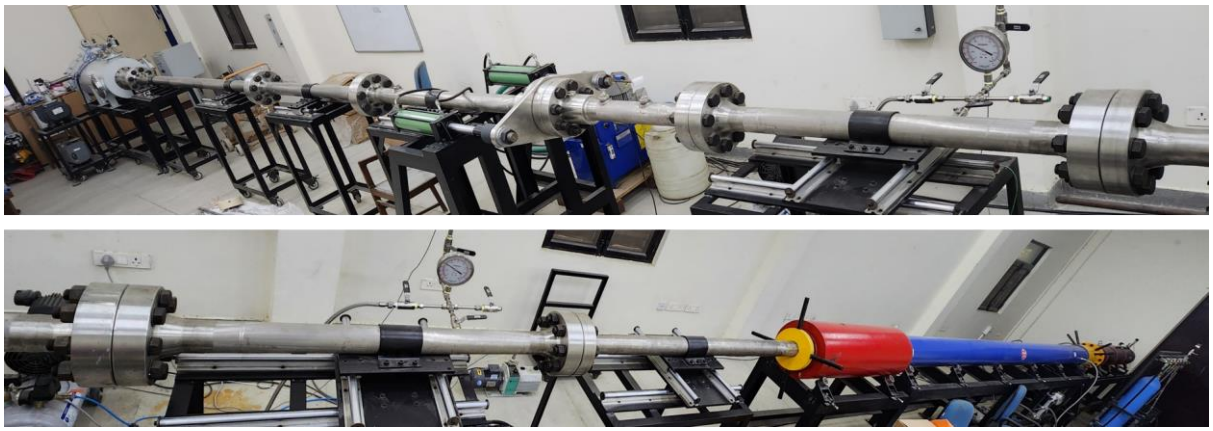

Fig 2. Image of Free Piston Type Expansion Tunnel (S2)

The expansion tunnel is operated by initially filling compressed air in the reservoir. When the valve is opened, high pressure air moves the piston in the driver section and it compresses the driver gas. When the pressure in the driver section reaches the bursting pressure of the primary diaphragm, it bursts. Maximum attainable pressure in the driver depends on the initial fill pressure of the driver and reservoir while diaphragm bursting pressure depends on the thickness of the diaphragm. For repeatability, the diaphragm is scored with cross-shaped groove. Primary diaphragm before and after rupture is shown in Fig. 3. When attainable pressure in the driver tube is lower than the diaphragm bursting pressure, it does not burst and when attainable pressure is much higher than the bursting pressure, Piston may collide with the buffer at another end of the tube with very high velocity. It may damage the piston and facility So it is very necessary to predict the initial pressure of gas in the reservoir and driver tube.

Fig 3. Primary Diaphragm (Left: Before rupture, Right: After rupture)

When the primary diaphragm bursts, a shock wave is generated which travels in the shock tube and processes the test gas to the state 2. The secondary diaphragm bursts on contact with the shock wave.

This shock wave then accelerates as it passes low pressure gas in acceleration tube at constant velocity. Test gas follows the shock wave and accelerates through unsteady expansion into state 7. At the nozzle, the test gas undergoes steady expansion to reach its final state (state 8). The test time is the period of steady flow following the arrival of the test gas-acceleration gas interface at the test section, as shown in the x-t diagram in Fig. 1. Test time may end with the arrival of the test gas's expansion or wave reflected off the driver-test gas interface.

The performance of the Expansion Tunnel is measured based on the flow property of the test gas in the test section and test time. It is influenced by the type of gas and the initial filling pressure inside the driver tube, shock tube, and acceleration tube. This gives a large degree of freedom to generate various flow conditions in the Expansion Tunnel. This facility can also be operated in Shock tunnel mode. In this mode, a secondary diaphragm is used at the nozzle inlet. This makes the total length of the shock tube section 12.5 m. In the present study, only the Expansion tunnel mode of this facility is used. This facility has several sensor tappings at various sections. There is one sensor at the end of the driver tube, three sensors in the shock tube, and four sensors in the acceleration tube. The location of sensors in the facility and their notations are shown in Table 2.

Table 2. Sensor location on FPET

Sensor distance from primary diaphragm (mm)	Sensor name	Facility section
-156	d1	Driver tube
3867	s1	Shock tube
4147	s2	Shock tube
4387	s3	Shock tube
6186	a1	Acceleration tube
6471	a2	Acceleration tube
12106	a3	Acceleration tube
12396	a4	Acceleration tube

For data acquisition during experiments, the NI USB 6356 Multifunction I/O data acquisition device was used. The sampling rate of data acquisition was 1 million samples/s per channel. Data was collected for 0.3 s after the data acquisition system was triggered by the driver sensor (d1). The pressure sensors which were used during experiments are PCB model 113B24 pressure sensor. For flow visualization Chronos 1.4 High speed camera was used.

3. Results and Discussion

3.1. Maximum attainable pressure in the driver

As described in Section 2, the rupture pressure of the diaphragm depends on the thickness of the primary diaphragm. Diaphragm burst only when attainable pressure in the driver is greater than diaphragm bursting pressure. To find the operating conditions of FPET, test runs were conducted with fill conditions mentioned in Table 3.

Pressure in the driver tube was measured using PCB pressure transducer fitted in sensor tapping at the end of the driver tube. Instantaneous Driver Pressure measured in one of the runs is shown in Fig. 4. From this figure, it can be found that the maximum attainable pressure in the driver is 92 bar.

Table 3. Operating conditions of FPET test run

Reservoir Condition	20 bar N_2
Driver Condition	0.9 bar Air
Shock Tube Condition	11 kPa Air
Acceleration Tube Condition	100 Pa Air
Primary Diaphragm	2.25 mm scored Aluminium diaphragm
Secondary diaphragm	50 μm Mylar diaphragm

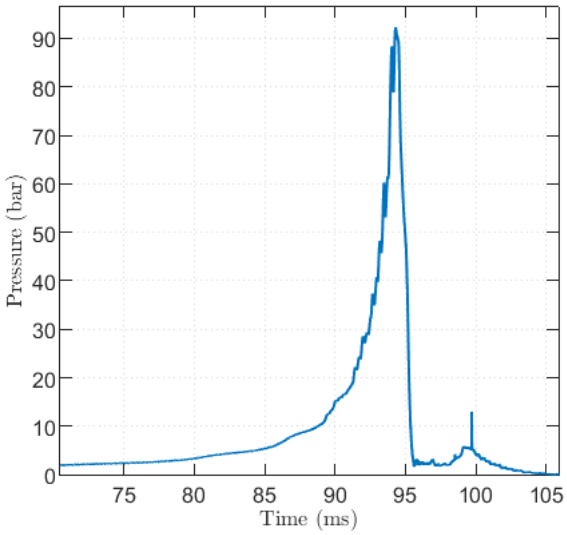

Fig 4. Instantaneous Pressure in Driver Tube

To know if piston velocity was very high at the time of impact on the buffer, the buffer condition was checked after each run. If the buffer is damaged heavily then that fill condition is discarded. Buffer condition after a test run is shown in Fig. 5. From Fig. 5, it can be seen that after the piston impacts on buffer, it is not severely damaged and there is only a slight impression of the piston on it. From this, it can be deduced that the piston impact velocity on the buffer was small which is suitable for operating the facility in this condition.

Fig 5. Teflon buffer after a test run

3.2 Determination of shock speeds in shock tube and acceleration tube

Fig. 6 shows the instantaneous pressure signals obtained using PCB pressure transducer in the shock tube and acceleration tube. Using the distance between sensors and the time duration needed for the shock to travel between sensors, Shock speed is calculated. The calculated shock speed between various sensors in the shock tube and acceleration tube is shown in Table 4.

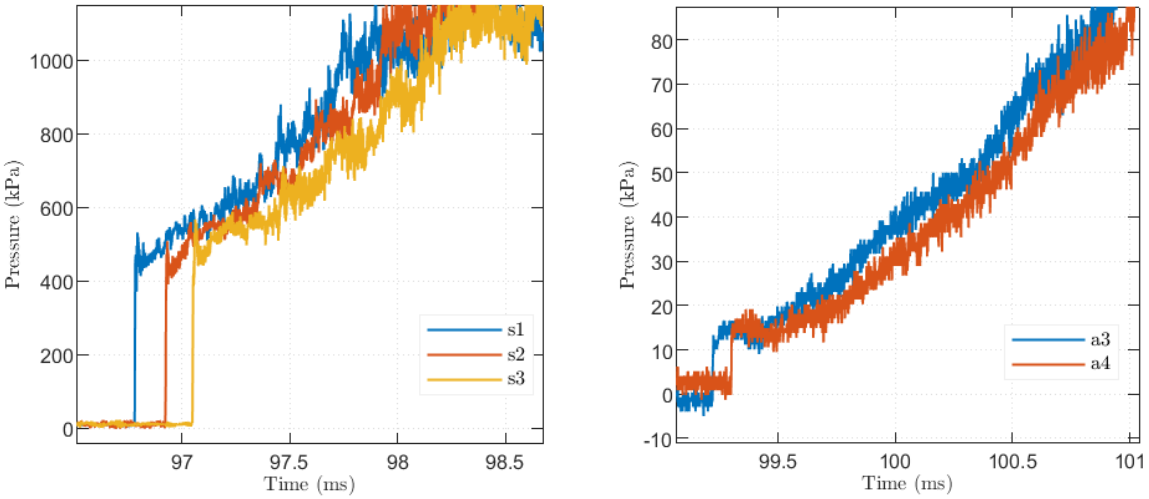

(a) Pressure in shock tube (b) Pressure in acceleration tube

Fig 6. Instantaneous pressure in shock tube and acceleration tube sensors

Table 4. Experimentally measured shock speeds for the test run mentioned in Table 3

Shock Tube shock speeds ($V_{s,1}$)	
Shock speed between s1 and s2 (m/s)	1958
Shock speed between s2 and s3 (m/s)	1920
Shock speed between s1 and s3 (m/s)	1948
Average shock speed (m/s)	1942
Acceleration tube shock speeds ($V_{s,2}$)	
Shock speed between a1 and a2 (m/s)	3851
Shock speed between a3 and a4 (m/s)	3766

The average shock speed of the Primary shock wave in the shock tube is used for the calculation of the properties of test gas in various states (shown in Fig. 1) whereas shock speed between sensors a3 and a4 has been used in calculations as both these sensors are very near to nozzle and sensors a1 and a2 are very far from sensors a3 and a4 as mentioned in Table 2. These shock speed are used in calculating the pressure and velocity of shock-processed test gas and shock-processed acceleration gas.

3.3 Calculation of freestream properties

Freestream properties (Mach no., temperature, pressure, density, etc.) are calculated using shock speeds and static pressure in the shock tube and acceleration tube and pitot pressure (stagnation

pressure behind the normal shock wave) in the test section[10]. Instantaneous Pitot Pressure is given in Fig. 8.

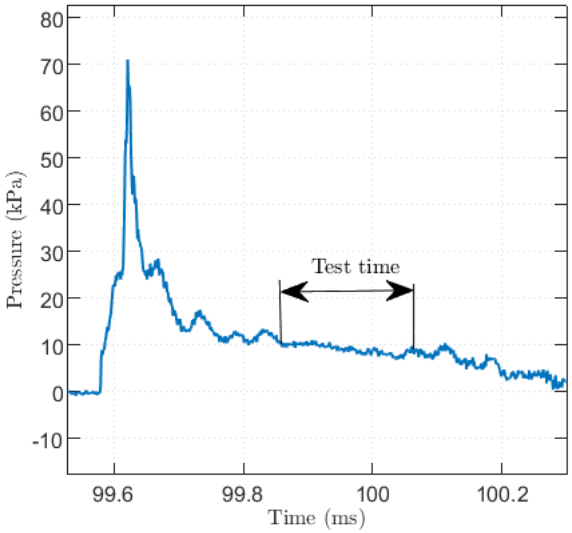

Fig 7. Instantaneous Pitot Pressure

Due to the primary shock wave in the shock tube, test gas is processed from state-1 to state-2 (see x-t diagram in Fig. 1). Properties (temperature, pressure, etc.) in state-2 can be calculated using Normal shock relations. Due to shock waves, secondary diaphragm ruptures. When the ideal case is assumed, the effects of the secondary diaphragm are not considered during and after its rupture as shown in Fig. 1. But in reality, the diaphragm hold time, its inertia, and its breakage affect the overall condition.

To consider the effect of the diaphragm, one model is the inertial diaphragm model[11]. This model assumes that the diaphragm breaks along its periphery and moves along the flow. Initially, it stagnates the test gas behind it which creates a reflected shock in the shock tube. Then it accelerates in the acceleration tube acting as a piston to acceleration tube gas. As the diaphragm accelerates, it reduces the strength of the reflected shock wave till it becomes a Mach wave. In his model, Petrie-Repar[12] used an initially curved diaphragm which later broke into 7 or 14 pieces. This model does not include diaphragm hold time and viscous effects. Another model is the hold time model which assumes that when a shock wave hits the diaphragm, the diaphragm remains closed for some duration (called hold time) due to which some test gas is processed by the reflected shock wave and then the diaphragm ruptures and its effects in the flow is not considered after that. Due to very less test runs, the effects of diaphragm rupture were not considered in this study and all the calculations were done using an ideal case in which it is assumed that the effects of the diaphragm do not exist after its rupture. However, some kind of inertial diaphragm model is planned to be included in the future for the calculation of free stream properties.

Properties (temperature and pressure) of acceleration gas after processing by secondary shock wave (state-6) is found using normal shock relations. Shock-processed test gas is unsteadily expanded from state 2 to state 7. Test gas temperature in state 7 is calculated assuming isentropic flow from state 2 to state 7. γ_2 is used in isentropic relation considering frozen thermochemistry across unsteady expansion. γ_2 is calculated from Gaseq chemical equilibrium program[13]. As there is a contact surface between state 6 and state 7, test gas is expanded such that $V_7 = V_6$ and $p_7 = p_6$. However, due to low density in the acceleration tube, Mirels' effect must be considered[14][15]. According to Mirels, low density boundary layer effects become more prominent when acceleration tube fill pressure (p_5) is less than 133 Pa (1 torr). As in our study, the fill pressure in the acceleration tube is less than this pressure, and Mirels' effect becomes important. In Mirels's effect, test gas is expanded further than what was expected from basic shock tube theory due to the boundary layer. In the limiting case of the Mirels effect, test gas expands to secondary shock wave velocity ($V_{s,2}$) as shown in Fig. 8. In reality, velocity (V_7) should lie between these two theoretical limits ($V_7 = V_6$ and $V_7 = V_{s,2}$). In the present study, a limiting case of Mirels effect is considered.

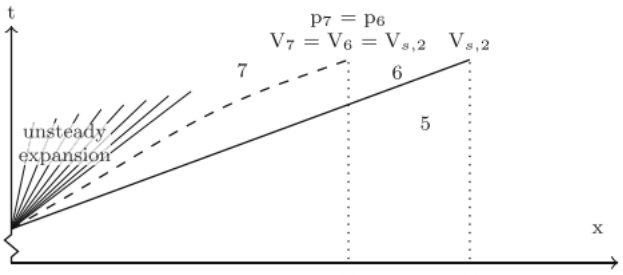

Fig 8. Overexpansion in acceleration tube[10]

After unsteady expansion, test gas undergoes steady expansion in the nozzle from state 7 to state 8. The geometric area ratio of the nozzle is 9.47. However, freestream flow obtained using this area ratio does not represent accurate flow. As the nozzle in the expansion tunnel is supersonic, test gas that passes through the nozzle has a boundary layer that is developed through the acceleration tube[10]. The effect of this boundary layer inside the nozzle can be modeled using the effective area ratio for this nozzle as shown in Fig. 9. From the literature[15], it is observed that only pressure and stagnation enthalpy are most affected by nozzle effective area. To find the effective area ratio tailored for each operating condition, extensive experimentation is needed hence in the current study only the geometric area ratio is considered in steady expansion.

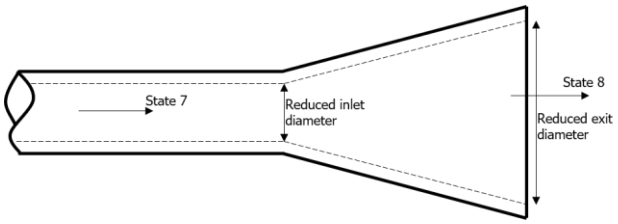

Fig 9. Representation of Boundary layer in nozzle (not to scale)

Table 5. Freestream properties for the test run mentioned in Table 3

Freestream Properties (at the nozzle exit, using an area ratio of 9.47)	
Freestream Mach No.	9.46
Freestream Velocity (m/s)	3921
Freestream Static Pressure (Pa)	662
Freestream density (Kg/m^3)	0.005155
Freestream Temperature (K)	447
Stagnation Enthalpy (MJ/Kg)	8.145
Test time (μs)	190

Calculated Freestream conditions are mentioned in Table 5. Test time is found using pitot pressure obtained in the test run. The measured test time was 190 μs. Test flow velocity was found to be 3.921 km/s and stagnation enthalpy is 8.145 MJ/kg. The main sources of uncertainty in the freestream conditions are shock speed calculation, primary diaphragm model, Mirels' effect consideration, and effective area ratio consideration. Uncertainty related to Diaphragm models, Mirels' effect, and effective nozzle area can only be minimized after extensive experimentation.

3.4 Flow Visualization

Flow visualization was done using Chronos 1.4 High speed camera. The frame rate of the camera was set at 7000 fps. Fig. 10 shows the images obtained during the test run. The time interval between each image is 140 µs. Fig. 10(a) is just before starting of the flow. Fig. 10(b), and (c) are images of flow with acceleration tube gas and Fig. 10(d), (e) are images of flow with test gas. Fig. 10 (f) is after the end of test time. During the test time radiation emission was observed.

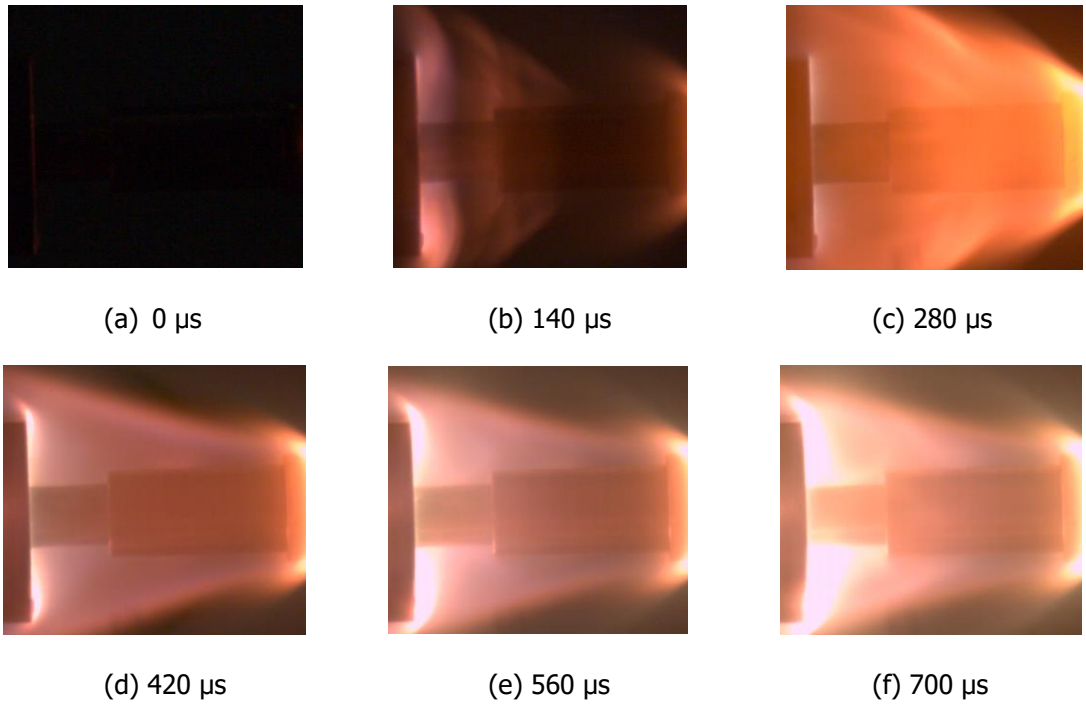

(a) 0 µs (b) 140 µs (c) 280 µs

(d) 420 µs (e) 560 µs (f) 700 µs

Fig 10. Flow visualization using High-Speed Camera

4. Conclusion

Free Piston type expansion tunnel has been developed for superorbital re-entry flows. It has a test section with 0.2 m nozzle exit diameter. High-frequency pressure measurements have been done using PCB pressure transducer. Flow visualization has been done with the help of high-speed camera. One operating condition of the expansion tunnel was characterized. Using the primary and secondary shock speed, pitot pressure and initial operating conditions of FPET test run, freestream conditions have been calculated. During the calculation, the effect of the diaphragm model, and nozzle effective area are neglected due to limited experimentation. And limiting case of Mirel's effect is considered. During test time, the emission of radiation has been observed.

In the future, more operating conditions will be developed for both expansion tunnel and shock tunnel mode of Free piston type expansion tunnel. Extensive experimentation is needed to find the actual core flow region and test flow disturbances. Radiation emitted during test runs is also needed to be studied to investigate the thermochemical nonequilibrium phenomenon.

Acknowledgment

The authors acknowledge the financial support provided by the Aeronautical Research and Development Board (ARDB), DST-FIST and Indian Institute of Technology, Kanpur for the development of Free Piston Type Expansion Tunnel (S2).

References

1. LYNE, J.E., TAUBER, M.E. and BRAUN, R.D. Parametric study of manned aerocapture Part I: Earth return from Mars, J Spacecr Rockets, November-December 1992, 29, (6), pp 808
2. Resler, E. L., and D. E. Bloxsom.: Very high Mach number flows by unsteady flow principles, Cornell University Graduate School of Aeronautical Engineering, Limited Distribution Monograph (1952).
3. Robert L. Trimpi.: A preliminary theoretical study of the expansion tube, a new device for producing high-enthalpy short-duration hypersonic gas flows. NASA Technical Report R-133, 1962
4. Miller, C.G., Jones, J.: Development and performance of the NASA Langley Research Center expansion tube/tunnel, a hypersonic hypervelocity real-gas facility. In: The 14th International Symposium on Shock Waves, Sydney, NSW, Australia (1983)
5. Stalker, R. J.: The Free-Piston Shock Tube, The Aeronautical Quarterly, 17 (1966), pp. 351–370
6. Stringer, I.: "TQ" free piston expansion tube-design and operation. Report 4/1989, Department of Mechanical Engineering, The University of Queensland, Brisbane, Australia (1989)
7. Doolan, Con. "Design and construction of the X-2 two-stage free piston driven expansion tube." Shock Tunnel Studies of Scramjet Phenomena 1994 (1995).
8. Dufrene, Aaron, Manu Sharma, and J. M. Austin. "Design and characterization of a hypervelocity expansion tube facility." Journal of Propulsion and Power 23, no. 6 (2007): 1185-1193.
9. Abul-Huda, Y., Gamba, M.: Design and characterization of the Michigan hypersonic expansion tube facility (MHExT). In: 53rd AIAA Aerospace Sciences Meeting, Kissimmee, Florida, USA, January 5–9, AIAA Paper 2015-1785 (2015). doi:10.2514/6. 2015-1785
10. James, C. M., D. E. Gildfind, S. W. Lewis, R. G. Morgan, and F. Zander. "Implementation of a state-to-state analytical framework for the calculation of expansion tube flow properties." Shock Waves 28 (2018): 349-377.
11. Morgan, R., Stalker, R.: Double diaphragm driven free piston expansion tube. In: The 18th International Symposium on Shock Waves, Sendai, Japan, July 21–26 (1991)
12. Petrie-Repar, P.: Numerical simulation of diaphragm rupture. Ph.D. Thesis, University of Queensland, St. Lucia, Australia (1997)
13. Morley, Chris. "Gaseq: a chemical equilibrium program for Windows." *Ver. 0.79* (2005).
14. Mirels, H.: Test time in low-pressure shock tubes. Phys. Fluids 6, 1201–1214 (1963). doi:10.1063/1.1706887
15. Mirels, H.: Shock tube test time limitation due to turbulent-wall boundary layer. AIAA J. 2, 84–93 (1964). doi:10.2514/3.2218
16. MATLAB version: 9.8.0.1451342 (R2020a), Natick, Massachusetts: The MathWorks Inc.; 2020